DC Power-Line Communication Based on Power/Signal Dual Modulation in Phase Shift Full-Bridge Converters

Jin Du, *Student Member, IEEE*, Jiande Wu, *Member, IEEE*, Ruichi Wang, Zhengyu Lin, *Senior Member, IEEE*, and Xiangning He, *Fellow, IEEE*

***Abstract*—For intelligent dc distributed power systems (DC-DPSs), data communication plays a vital role in system control and device monitoring. To achieve communication in a cost-effective way, power/signal dual modulation (PSDM), a method that integrates data transmission with power conversion, can be utilized. In this paper, an improved PSDM method using phase shift full-bridge (PSFB) converter is proposed. This method introduces a phase control-based freedom in the conventional PSFB control loop to realize communication using the same power conversion circuit. In this way, decoupled data modulation and power conversion are realized without extra wiring and coupling units, and thus, the system structure is simplified. More importantly, the signal intensity can be regulated by the proposed perturbation depth, and so this method can adapt to different operating conditions. Application of the proposed method to a DC-DPS composed of several PSFB converters is discussed. A 2kW prototype system with an embedded 5 kbps communication link has been implemented, and the effectiveness of the method is verified by experimental results.**

***Index Terms*—DC distributed power system (DPS), phase shift full bridge, power-line communication, power/signal dual modulation.**

I. Introduction

DURING the past decades, distributed power systems (DPS) have experienced substantial development. The driving force of this comes from emerging power electronic applications including LED lightening, electric vehicle, and photovoltaic (PV) system [1], [2]. Compared with ac counterparts, DC-DPSs have advantages of simple structure with fewer conversion stages, and no need for phase or reactive power control [3], [4]. These merits make DC-DPS suitable for applications such as data center power supply systems and renewable generation systems.

In a DC-DPS, a number of different generation, storage, and consumption devices are connected to a common dc bus [5].

Manuscript received September 10, 2015; revised December 13, 2015; accepted February 3, 2016. Date of publication February 11, 2016; date of current version September 16, 2016. This work was supported by the National Nature Science Foundation of China under Grants 61174157 and 51577170 and by the Lite-On Power Electronics Technology Research Fund. Recommended for publication by Associate Editor J. A. Oliver.

J. Du, J. Wu, R. Wang, and X. He are with the College of Electrical Engineering, Zhejiang University, Hangzhou 310027, China (e-mail: eedujin@zju.edu.cn; eewjd@zju.edu.cn; rui_chi@163.com; hxn@zju.edu.cn).

Z. Lin is with the Department of Electronic and Power Engineering, Aston University, Birmingham B4 7ET, U.K. (e-mail: z.lin@ieee.org).

Color versions of one or more of the figures in this paper are available online at http://ieeexplore.ieee.org.

Digital Object Identifier 10.1109/TPEL.2016.2527739

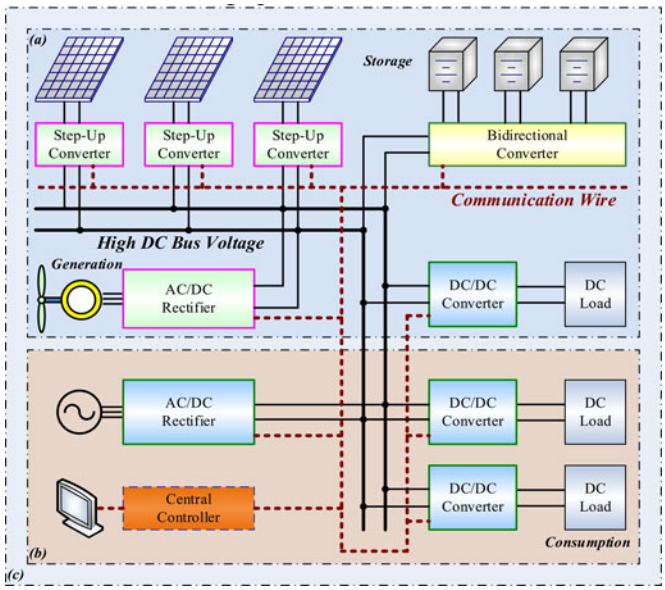

Fig. 1. Structures of different dc power system: (a) DG, (b) HVDC, and (c) microgrid.

Related topics, including distributed generation (DG) [6]–[9], high-voltage dc (HVDC) systems [10]–[12], and microgrids (MGs) [13]–[15] are the combination of some or all of the components mentioned earlier and have been widely discussed. Possible DC-DPS are shown in Fig. 1. In these systems, two schemes are commonly used for dc-bus voltage regulation: master–slave control and droop control [16]–[19]. In master–slave control, the master converter regulates the dc-bus voltage via a communication link and dependent upon the speed and reliability of the communication link. In a conventional droop control, the relationship between voltage and current is determined by fixed droop characteristic, such that the total power is balanced without communication. However, the dc-bus voltage shifts in different conditions, depending on the location of the converters and the length of the wire. To increase the accuracy of the dc-bus voltage control, low speed communication is incorporated into the improved droop control. Consequently, data communication is essential to build a high-performance DC-DPS.

Conventionally, wired communication technologies such as CAN and RS-485 have been widely used and proved to be reliable solutions. However, additional communication cable increases installation cost and system complexity. In recent years, wireless communication methods, such as Wi-Fi and Zigbee,

have been applied in control systems. It is attractive to eliminate additional communication cable. However, the reliability of wireless communication is often doubted, because it is susceptible to environment and vulnerable to attack.

Power line communication (PLC), which does not require additional communication cables, is a popular approach in ac system. In [20], a PLC-based communication architecture for an LVDC system is presented, which employs high-frequency (HF) PLC for monitoring, control and protection. It demonstrates that PLC is applicable to DC-DPS. However, according to European CENELEC standard EN 50065, narrow-band PLC (NB-PLC) is used for remote control and the carrier frequency of HF PLC is beyond the limitation of the standard.

For NB-PLC applied in a dc system, there are two constraints. First, the spectrum overlaps with the harmonics produced by power electronic converters, and consequently, communication is vulnerable to the switching frequency noise. Second, the capacitance of the dc-bus is large, varying from 10 μF to several mF, and so relatively high-power coupling circuits are required. Overall, the application of NB-PLC in DC-DPS is a challenge [21].

The power/signal dual modulation (PSDM) concept proposed in [22] provides possible method of achieving NB-PLC in DC-DPS. It embeds signals into power conversion by shifting the frequency of the switching power supply intrinsic harmonic. However, this method is based on basic PWM converters, and the signal intensity cannot be regulated.

To realize data communication in a DC-DPS consisting of several phase shift full-bridge (PSFB) converters while overcoming the aforementioned constrains, an improved NB-PLC approach based on PSDM is proposed in this paper. This method utilizes another freedom in conventional power control loop of the PSDM converter, to embed data modulation into power conversion. Two theoretically distinct modulation strategies, which are frequency-based and phase-based, respectively, are studied and compared. Then the proposed phase modulation is analyzed in detail. In addition, the concept of perturbation depth is proposed to describe the signal intensity regulation. The proposed method has the merits of decoupled control, adjustable signal intensity, and simplified hardware, and it has been verified by simulation and prototype experiment.

This paper is arranged as follows. The classification and evaluation of the modulation methods are presented in Section II. The principle of the phase modulation is analyzed in detail in Section III. Simulation verification and prototype experiment are shown in Section IV. Finally, conclusions are given in Section V.

II. Classification and Evaluation of Modulation Methods

In conventional power electronics converters, high-frequency harmonics at frequencies up to several hundreds of kilohertz are considered useless and introduce negative effects including decreased the power quality, degraded EMC, and so on. However, high-frequency signal can be utilized as data carrier. In conventional power-line communication systems, signal coupling

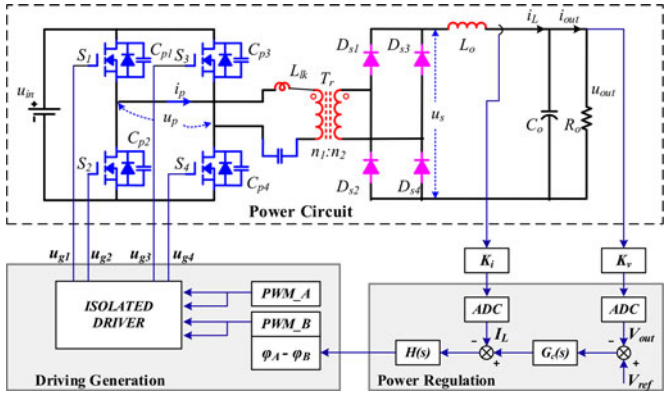

Fig. 2. Topology of a PSFB converter.

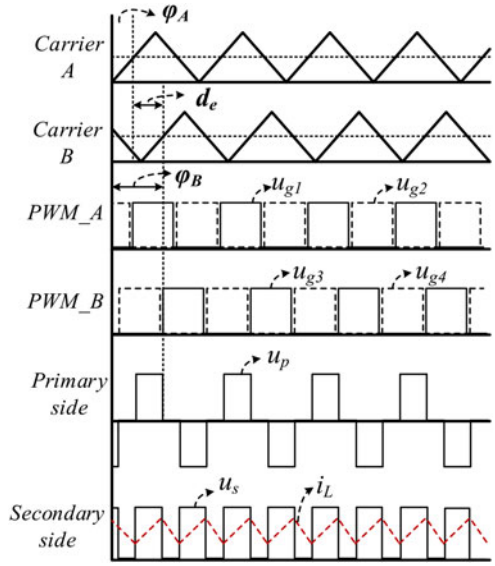

Fig. 3. Key waveforms of a PSFB converter.

circuits, which increases the system complexity and cost, are employed to inject high-frequency carrier into the power line. The principle of the PSDM method is to utilize the intrinsic harmonic produced by power electronic converter as data carrier. Thus, data modulation can be achieved without the coupling units in conventional PLC.

Phase shift full bridge (PSFB) is a popular topology, which has been widely applied in DC-DPS. By taking the advantage of intrinsic capacitor and leakage inductance, zero voltage switch (ZVS) can be realized to improve the efficiency. The circuit model and control strategy have been analyzed comprehensively [23]–[26].

A typical circuit structure and a digital control scheme of a PSFB converter are shown in Fig. 2, and the key waveforms are shown in Fig. 3. This circuit is controlled by a digital signal processor (DSP), in which two PWM generator modules are assigned to the leading leg and lagging leg, respectively, producing four gate drive signals. In this section, the methods of inserting information into PWM signal but without influencing the power output are discussed in detail.

In general, a triangular carrier is employed in PSFB circuit. The normalized triangular waveform is defined as

$$u_{\mathrm{tri}}(t)=\begin{cases}\dfrac{t\,\mathrm{MOD}\,2\pi}{\pi}, & 0\le(t\,\mathrm{MOD}\,2\pi)<\pi\\ 2-\dfrac{t\,\mathrm{MOD}\,2\pi}{\pi}, & \pi\le(t\,\mathrm{MOD}\,2\pi)<2\pi\end{cases}. \quad (1)$$

In a digital PWM module, the virtual waveform of a typical triangular carrier u_c can be expressed as

$$u_c(t)=u_{\mathrm{tri}}(2\pi ft+\varphi) \quad (2)$$

where f and φ are the frequency and phase angular of the carrier, respectively. These two parameters can be controlled. The other essential parameter is duty cycle d, which is set constantly to 1/2 by comparing the carrier wave with a dc reference set at 1/2.

Suppose the parameters in the two PWM modules corresponding to the leading leg and lagging leg are f_A, d_A, φ_A and f_B, d_B, φ_B, respectively. It is required that

$$f_A = f_B = f \quad (3)$$

$$d_A = d_B = 0.5 \quad (4)$$

$$\varphi_B-\varphi_A = d_e\pi\ (0<d_e<1) \quad (5)$$

where $\boldsymbol{d_e\pi}$ is the phase shift between the leading leg and lagging leg and regulates the output ratio of voltage pulse. The output voltage of the PSFB circuit is

$$U_{\mathrm{out}}=n\boldsymbol{d_eU_{dc}} \quad (6)$$

where n is turns ratio of transformer T_r and U_{dc} is the input voltage.

Equations (3)–(5) are the basic equations for the control of power conversion in a conventional PSFB circuit. However, in these equations, two freedoms can be exploited to transmit information, which will not affect power conversion. It is clear that the carrier frequency $\boldsymbol{f}$ can be a variable in order to embed signal. Equation (5) indicates that the relative phase between the leading leg and lagging leg $\varphi_B-\varphi_A$ is determined by power control. However, by defining the differential phase and the common phase as

$$\varphi_d = \frac{\varphi_B-\varphi_A}{2}$$

$$\varphi_c = \frac{\varphi_B+\varphi_A}{2} \quad (7)$$

then φ_A and φ_B can be expressed as

$$\varphi_A = \varphi_c-\varphi_d$$

$$\varphi_B = \varphi_c+\varphi_d. \quad (8)$$

It can be seen that the common phase φ_c is a decoupled control freedom, which can be modulated to embed data. Fig. 4 presents the aforementioned two methods by modulating f and φ.

A. Switching Frequency Shift Modulation

According to the aforementioned analysis, the switching frequency $\boldsymbol{f}$ is irrelevant to the power control algorithm, which means the frequency is a control freedom to carry information. To modulate information into the switching ripple, a common approach is frequency shift keying (FSK), as depicted as Method 1 in Fig. 4.

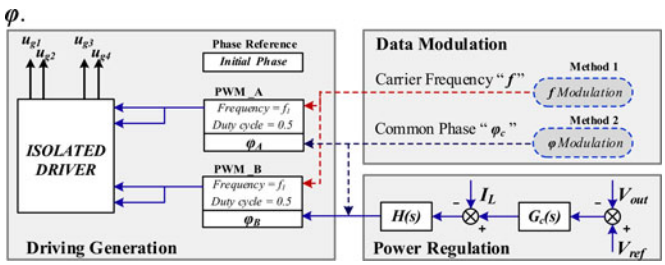

Fig. 4. Control scheme of a PSFB converter.

In a binary FSK strategy for example, the circuit operates at frequency $\boldsymbol{f_1}$ or $\boldsymbol{f_2}$ decided by the data to be sent. The modulated carrier can be expressed as

$$u_c(t)=\begin{cases}u_{\mathrm{tri}}(2\pi f_1t), & \text{when sending data "}\mathbf{0}\text{"}\\ u_{\mathrm{tri}}(2\pi f_2t), & \text{when sending data "}\mathbf{1}\text{"}\end{cases}. \quad (9)$$

In this way, data are injected into the converter. Rectified by a bridge in the secondary side, the circuit outputs a dc voltage with FSK-modulated ripple, whose fundamental harmonic is twice the carrier frequency. The fundamental harmonic of this dc voltage ripple is

$$f_s(t)=\begin{cases}A_1\sin 2\pi*2f_1t, & \text{when sending data "}\mathbf{0}\text{"}\\ A_2\sin 2\pi*2f_2t, & \text{when sending data "}\mathbf{1}\text{"}\end{cases}. \quad (10)$$

By adopting appropriate communication protocol, data can be modulated and transmitted.

B. Phase Shift Modulation

Phase shift keying (PSK) is a common method for data modulation. In a PSFB converter, the differential phase is relevant to power regulation, but the common phase can be modulated independently to implement data communication.

In such a scheme, the PWM carrier is no longer a pure triangular wave. To ensure the independence of power regulation and data communication, it is required that

$$u_A(t-T_d)=u_B(t) \quad (11)$$

where u_A and u_B are the carrier waves of the leading leg and lagging leg, respectively, and T_d is the delay time corresponding to the duty cycle of the power output.

Assume that in every period, carrier wave is a triangular wave with a data-modulated phase angular $\varphi(t)$. The modulated carriers of the leading leg and the lagging leg can be expressed as

$$u_{cA}(t) = u_{\mathrm{tri}}(2\pi ft+\varphi(t))$$

$$u_{cB}(t) = u_{\mathrm{tri}}(2\pi ft+d_e\pi+\varphi(t+d_e/2f)). \quad (12)$$

In a digital controlled system, the carrier phase is changed every period, so that $\varphi(t)$ can be expressed as a discrete series

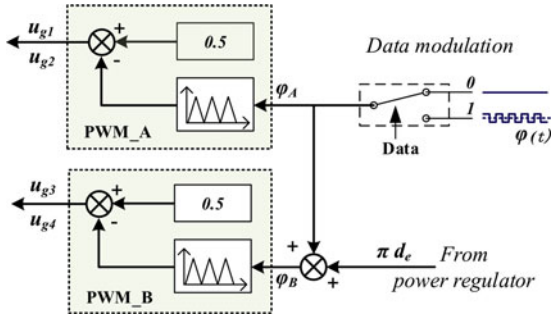

Fig. 5. Principle of the phase modulation.

$\varphi[n]$, the relationship between $\varphi(t)$ and $\varphi[n]$ is

$$\varphi(t) = \varphi(n/f) = \varphi[n] \tag{13}$$

where $n = \text{Int}(t \cdot f)$.

If $\varphi[n] = 0$, the circuit operated in conventional mode; otherwise, the data carrier can be introduced by selecting a proper digit sequence. The principle shown in Fig. 5 employs an on–off keying modulation with sequence $+\varphi$, $-\varphi$. In this way, designed frequency component can be injected into the converter. In receiver, the frequency component can be detected and demodulated as data "1."

Frequency modulation and phase modulation are essential modulation strategies, and both can be employed in PSDM systems. However, frequency modulation method has the drawback that the amplitude of the carrier is determined by the power regulator, and the signal intensity cannot be controlled independently, so it is unsuitable for long range communication. On the contrary, phase modulation strategy applied in PSFB converter is flexible. It not only provides an intensity-controllable approach to adapt to complex operation environment, but also avoids the signal intensity attenuation caused by power regulation. By selecting different digit sequence, different frequency carrier with variable amplitude can be produced.

III. Principle of the Phase Modulation

According to the analysis in Section II, phase modulation on PWM carrier is suitable for data communication applied in PSFB converters due to its merits.

A. Perturbation Process

In this section, the process of the data modulation is discussed.

The principle of the proposed method is to modulate the data signal into the carrier phase of legs. This paper employs a bipolar modulation method, which guarantees the average current unchanged with modulation. In this method, bit "1" is represented by alternative $+\Delta\varphi$ and $-\Delta\varphi$, while bit "0" is represented by no perturbation. A normalized bipolar square waveform is defined as

$$u_{\text{squ}}(t) = \begin{cases} 1, & 0 \le (t \,\text{MOD}\, 2\pi) < \pi \\ -1, & \pi \le (t \,\text{MOD}\, 2\pi) < 2\pi. \end{cases} \tag{14}$$

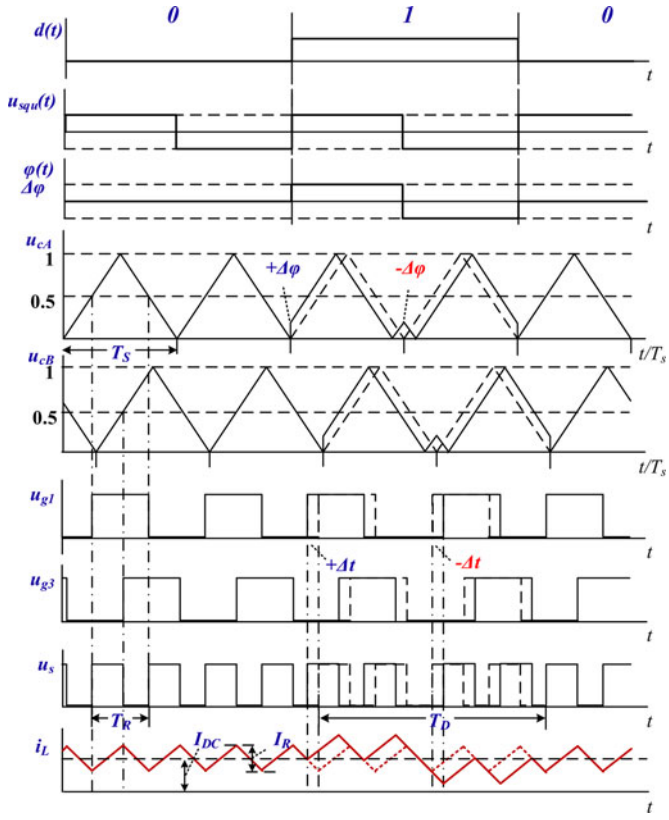

Fig. 6. Key waveform of the modulation process.

Letting the data sequence is $d(t)$, then the modulated phase shift can be expressed as

$$\varphi(t) = d(t) \cdot \Delta\varphi \cdot u_{\text{squ}}(2\pi f_2 t + \varphi_s) \tag{15}$$

where $\Delta\varphi$ is the amplitude of the phase perturbation, $\boldsymbol{f_2}$ is the perturbation frequency, and $\boldsymbol{\varphi_s}$ is the constant phase of the perturbation wave. The waveforms with the perturbation strategy are shown in Fig. 6.

Due to the phase perturbation, the waveforms of the carriers are altered. Graphically, that means the positive part of u_{g1} is delayed for $+\Delta\boldsymbol{t}$ or $-\Delta\boldsymbol{t}$ according to $\varphi(t)$, while u_{g3} remains a constant phase shift angle relevant to u_{g1}, where

$$\Delta t = \frac{\Delta\varphi}{\pi} * \frac{T_s}{2} = \frac{\Delta\varphi}{2\pi f_s}. \tag{16}$$

In this way, a data carrier, whose period is an integer multiple of the switching period, is injected, and it can be decomposed in the output voltage.

B. Analysis of the Spectrum with Perturbation

As shown in Fig. 6, small phase perturbations $+\Delta\varphi$ and $-\Delta\varphi$, which cause the time displacement in the secondary voltage u_s and the inductor current i_L, are introduced to the carrier waveform; thus, the output spectrums are changed. To analyze the spectrum of u_s with the proposed modulation strategy, detailed analysis is given in this part.

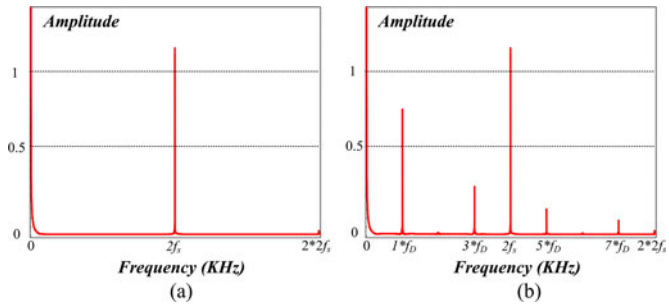

Fig. 7. Spectrum of transformer secondary voltage: (a) without data modulation and (b) with data modulation.

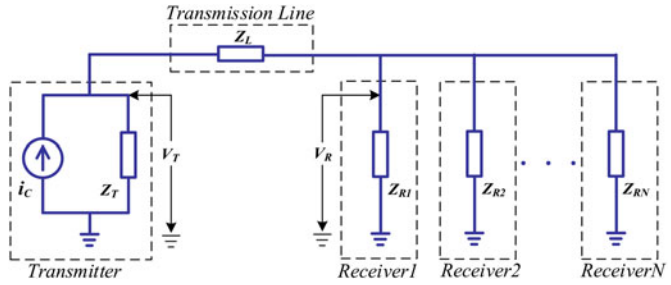

Fig. 8. Equivalent circuit of signal transmission.

A normalized pulse waveform u_{R0} is defined as

$$u_{R0}(t) = \begin{cases} 1, & 0 \le x < dT_R \\ 0, & x \ge dT_R. \end{cases} \tag{17}$$

For conventional PWM control, u_{R0} is extended in every T_R periods as u_R and it can be expressed as Fourier series

$$u_R(t) = \sum_{n=-\infty}^{\infty} C_n \cdot e^{jn\omega_0 t} \tag{18}$$

where

$$\begin{aligned} C_n &= \frac{1}{T_R}\int_0^{T_R} u_R(t)\, e^{-jn\omega_0 t} dt \\ &= \frac{1}{2\pi n}\sin 2\pi n \cdot d - j \cdot \frac{1}{2\pi n}(1-\cos 2\pi n \cdot d). \end{aligned} \tag{19}$$

Then the fundamental component u_{R1} is

$$u_{R1}(t) = \frac{2}{\pi} \cdot \sin \pi d \cdot \cos(\omega_0 t - \pi d). \tag{20}$$

For conventional PSFB converters, the output fundamental harmonic frequency $f_R = 1/T_R$ is twice the switching frequency f_s, and the spectrum is shown in Fig. 7(a).

According the analysis in the last section, the data are modulated in every $4T_R$ period, so the data-modulated pulse waveform u_{D0} can be expressed as

$$\begin{aligned} u_{D0}(t) &= (u_{R0}(t+\Delta t) + u_{R0}(t - T_R + \Delta t) \\ &\quad + u_{R0}(t - 2T_R - \Delta t) + u_{R0}(t - 3T_R - \Delta t)). \end{aligned} \tag{21}$$

Extending u_{D0} in every $4T_R$ periods, it can be expressed in Fourier series,

$$u_D(t) = \sum_{n=-\infty}^{\infty} C_m \cdot e^{jm\omega_D t} \tag{22}$$

where $\omega_D = \pi/2T_R$ and

$$\begin{aligned} C_m &= \frac{1}{4T_R}\int_0^{4T_R} u_{D0}(t)\, e^{-jm\omega_D t} dt \\ &= \frac{1}{4T_R}\int_0^{4T_R} [(u_{R0}(t+\Delta t) + u_{R0}(t - T_R + \Delta t) \\ &\quad + u_{R0}(x - 2T_R - \Delta t) \\ &\quad + u_{R0}(x - 3T_R - \Delta t)] e^{-jm\omega_D t} dt \\ &= \frac{1}{4T_R}[e^{j\omega_D \Delta t} + e^{j(-\frac{\pi}{2}) + j\omega_D \Delta t} + e^{j(-\pi) - j\omega_D \Delta t} \\ &\quad + e^{j(-\frac{3\pi}{2}) - j\omega_D \Delta t}] \int_0^{4T_R} u_{R0}(t)\, e^{-jm\omega_D t} dt \\ &= \frac{1}{2T_R}(1+j) \cdot \sin \omega_D \Delta t \Delta \int_0^{4T_R} u_{R0}(t)\, e^{-jm\omega_D t} dt. \end{aligned} \tag{23}$$

The fundamental frequency in (22) is utilized as data carrier and defined as f_D, where $f_D = f_s/2 = f_R/4$. By simplifying (23), the normalized voltage amplitude of the data carrier is

$$A_{D1} = |C_1| = \frac{4\sqrt{2}}{\pi}\sin\frac{\pi d}{4} \cdot \sin \omega_D \Delta t = k \cdot \sin \omega_D \Delta t. \tag{24}$$

It can be seen that due to the phase shift control strategy, a data carrier with frequency f_D has been introduced. The normalized amplitude of the frequency component at f_D is related to time displacement Δt. The spectrum is shown in Fig. 7(b).

C. Data Signal Intensity Control

For a DC-DPS combined with power-line communication, different operation circumstances should be considered. Considering a system that a transmitter converter is located in one end of the bus and the other receiver converters are located in the other end, the equivalent circuit of the signal transmission is shown in Fig. 8, where Z_T, Z_L, and Z_{Rn} are the impedances of the transmitter converter, the transmission line, and the receivers, respectively, and i_c is the data-carrier current source. The attenuation rate of the signal r_a is defined as

$$r_a = \left|\frac{V_R}{V_T}\right| = \left|\frac{1}{1 + Z_L \times \sum_{n=1}^{N}(1/Z_{Rn})}\right|. \tag{25}$$

It can be see that the data signals transmitted to the receivers are degraded with the increasing of the bus length and the converter number. To decode the data signal correctly, it is necessary to adjust the signal intensity according to the communication circumstance. Thus, perturbation depth δ is proposed to control the communication power.

According to (24), the normalized voltage amplitude of the data carrier is derived as $k \cdot \sin \omega_D \Delta t$. Note that $\omega_D = 2\pi/T_D$ and $\Delta t = \Delta\varphi/2\pi f_s$, so it can be written as $k \sin(\Delta\varphi/2)$.

When the power regulator operating in steady state, the equivalent duty cycle d_e of the converter is constant, then the data signal intensity is controlled by the phase perturbation $\Delta\varphi$. When $\Delta\varphi$ is small, $\sin(\Delta\varphi/2) \approx \Delta\varphi/2$, thus the amplitude of the voltage fundamental component can be written as $(k/2) \cdot \Delta\varphi$, and the amplitude of the data carrier of inductor current can be derived as

$$A'_D \approx \frac{\sqrt{2} \sin \pi d U_i \Delta\varphi}{\pi^2 K_T f_s L} \tag{26}$$

where U_i is the input voltage and K_T is the transformer ratio of the transformer.

The perturbation angular in a cycle is defined as perturbation depth δ

$$\delta = \frac{\Delta\varphi}{\pi}. \tag{27}$$

Equation (26) demonstrates that the amplitude of the signal carrier is about proportional to perturbation depth δ, so the intensity of the data signal can be regulated by δ. However, for the inductor current i_L shown in Fig. 6, it is necessary to ensure that the perturbed current in continuous mode. It should follow:

$$\Delta i < I_{\rm dc} - \frac{I_R}{2}. \tag{28}$$

If the aforementioned equation is not satisfied, the inductor current is forced into discontinuous mode by the phase modulation. In this case, the data carrier cannot be superimposed linearly to the bus, and it will affect the power regulation.

In continuous mode, the current difference is

$$\Delta i = \frac{U_L}{L} * \Delta t = \frac{-U_O}{L} * \frac{\Delta\varphi}{\pi f_s} \tag{29}$$

where the output voltage is

$$U_O = \frac{D U_i}{K_T}. \tag{30}$$

So

$$\Delta i = \frac{D U_i}{K_T L} * \frac{\Delta\varphi}{\pi f_s}. \tag{31}$$

According to (28)–(31), the limitation of the perturbation depth is derived

$$\delta < \left(I_{\rm dc} - \frac{I_R}{2} \right) * \frac{K_T L f_s}{D U_i}. \tag{32}$$

It can be seen from (31) to (32) that the maximum potential perturbation depth is limited by the dc current component. It means that the maximum amplitude of the output data carrier that the converter can send out has a positive linear relationship with the output power.

IV. Simulation and Experimental Verification

In this section, the phase modulation method is simulated by PSIM and implemented in a prototype system. Furthermore, data communication is realized between two 1 kW converters.

TABLE I
Specifications of the Prototype Converter

Parameter	Variable	Value/Model
Rated power	P	1 kW
Input voltage	$V_{\rm in}$	100 V
Output voltage	$V_{\rm out}$	100 V
Transformer ratio	K_T	6:9
Inductance	L	60 μH
Capacitor	C	470 μF
	ESR	50 mΩ
Power MOS	S	IPW65R037C6
Power Diode	D	C4D20120D

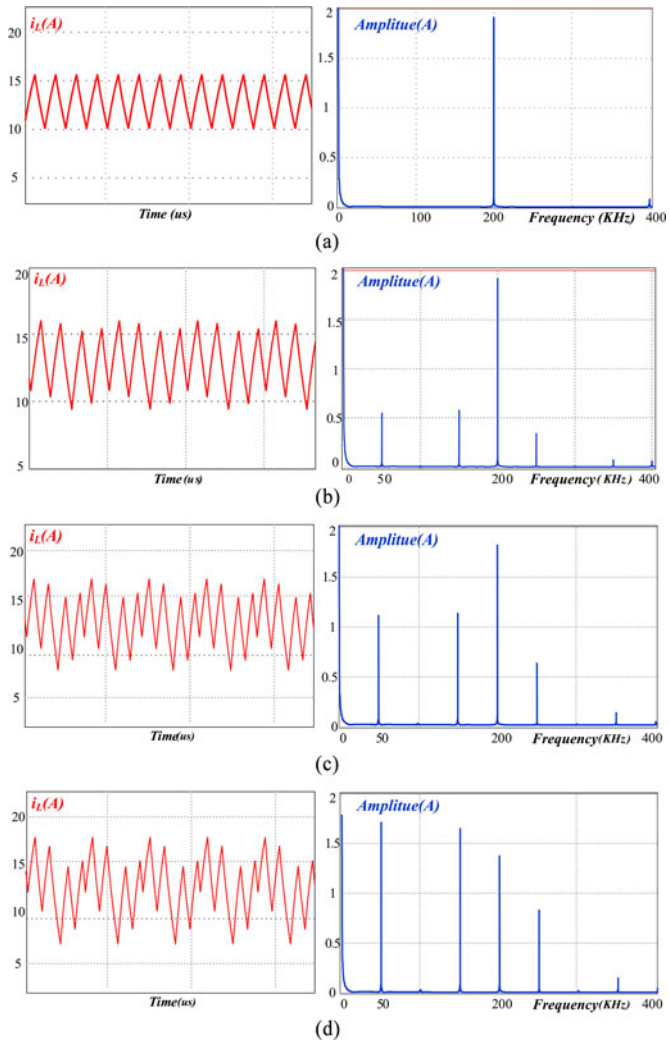

Fig. 9. Simulation result: current waveform and its spectrum: (a) with $\delta = 0$, (b) with $\delta = 0.05$, (c) with $\delta = 0.1$, and (d) with $\delta = 0.15$.

A. Simulation

A typical PSFB converter is established in PSIM, which complies with the specification listed in Table I. The carrier frequency is set 100 kHz. The output inductor current with different perturbation depth δ is sampled and the spectra are analyzed, which are shown in Fig. 9.

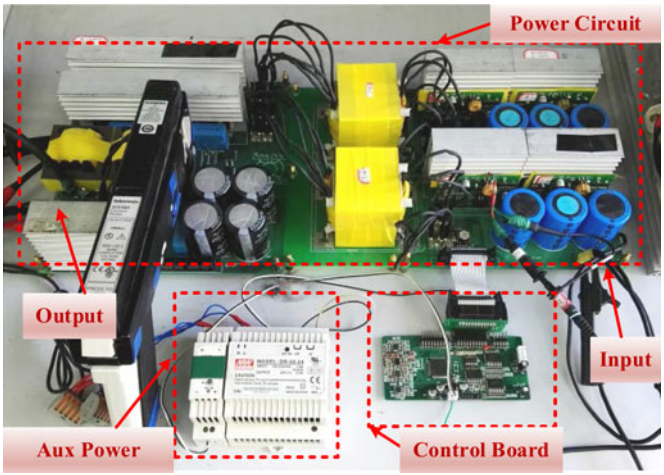

Fig. 10. Prototype.

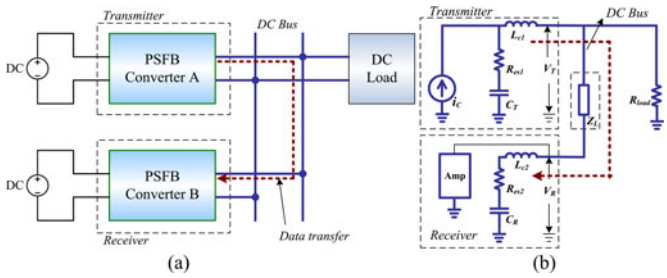

Fig. 11. Experiment system: (a) structure and (b) communication equivalent circuit.

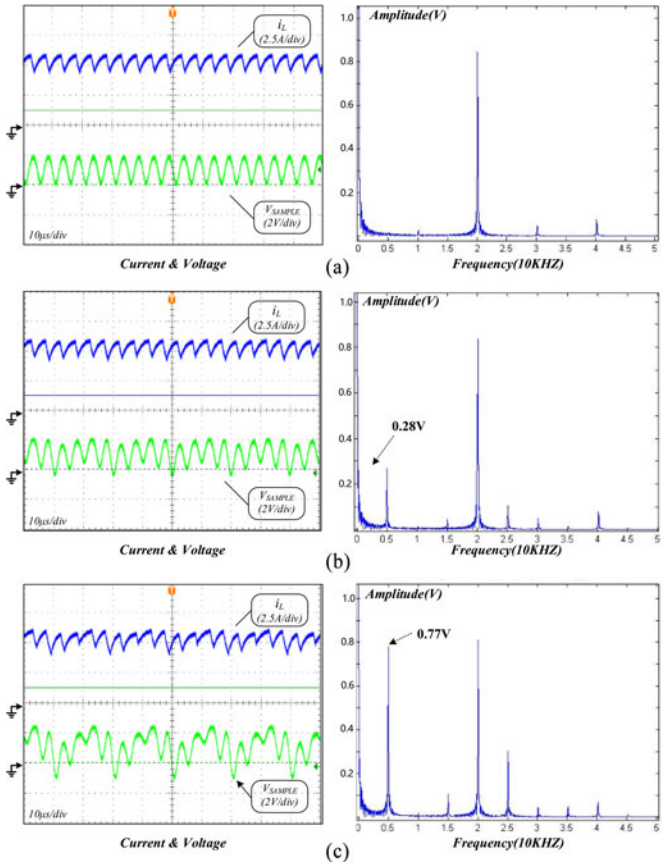

Fig. 12. Experiment result: waveform and spectrum, (a) with $\delta = 0$, (b) with $\delta = 0.04$, and (c) with $\delta = 0.11$.

In Fig. 9(a), it is clear that the data carrier frequency 50 kHz component does not exist when $\delta = 0$. The current is a triangle wave, and the dominating harmonic is the 200 kHz fundamental component. With the increasing of δ, the intensity of the data carrier frequency 50 kHz is promoted. When $\delta = 0.15$, as the analysis in Section III, the amplitude of the perturbation frequency component keeps increasing and exceeds the amplitude of the switching frequency component.

The simulation demonstrated is consistent with the theoretical analysis.

B. Prototype Experiment

To verify the proposed method experimentally, a prototype system composed of two PSFB converters is set up. The specification of the converter is listed in Table I, and the photo of a prototype converter is shown in Fig. 10.

Two experiments are carried out. The validity of the perturbation method is verified at first, and then the data decoding algorithm is tested. The verification system structure is shown in Fig. 11(a), and the equivalent circuit of the communication system is depicted in Fig. 11(b). In this system, one converter operates as a transmitter and the other operates as a receiver, and the output capacitor and its equivalent series resistor of these converters are C_T, C_R and $R_{\rm es1}$, $R_{\rm es2}$, respectively. To increase the input impedance of the converters, small inductors L_{c1} and L_{c2} with 5 μH inductance are added to the output line.

TABLE II
COMPARISON OF SIMULATION RESULT AND EXPERIMENT RESULT

Simulation			Experiment		
δ	Amplitude	p.u.	δ	Amplitude	p.u.
0	0	0	0	0	0
0.05	0.6	0.25	0.04	0.27	0.2
0.10	1.16	0.48	0.11	0.77	0.57
0.15	1.71	0.71	0.16	1.05	0.78

1) Perturbation Depth Verification: In this experiment, converter A sends out 50 kHz harmonics representing signal "1" continuously, and the inductor current of the converter is measured by a current probe. On the dc bus, a voltage ripple amplifier circuit whose gain is set 35.6 dB is employed to receive the modulated signal. Similar to the simulation process, the waveforms and voltage spectrum of the converter with different perturbation depth are recorded and analyzed in Fig. 12, where i_L is the inductor current and $V_{\rm Sample}$ is the output voltage ripple, which has been filtered and amplified.

The results of simulation and prototype experiments are summarized in Table II and depicted in Fig. 13. From the comparison, the approximately linear relationship between the perturbation depth and the amplitude of the data carrier is proved.

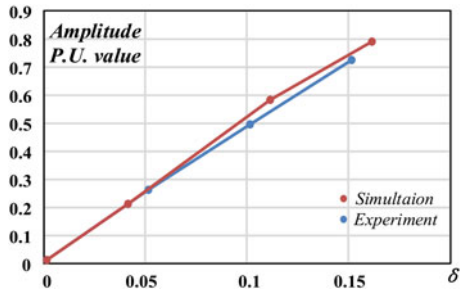

Fig. 13. Comparison of simulation result and experiment result.

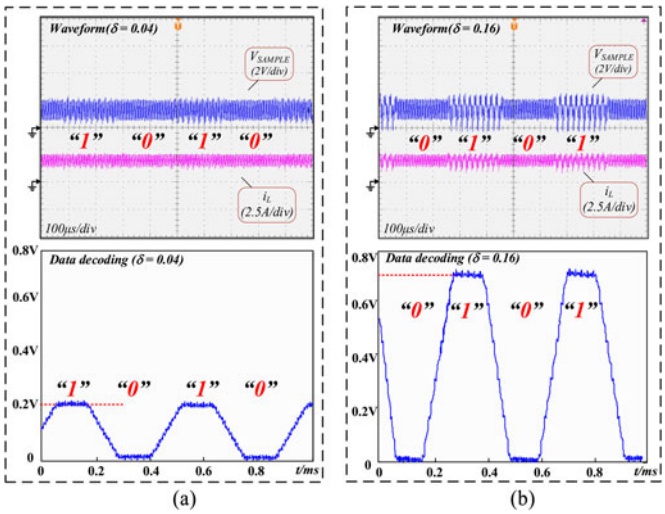

Fig. 14. Data decoding result: (a) with $\delta = 0.04$ and (b) with $\delta = 0.16$.

2) Communication Validity: The communication function is realized and tested based on the verification system shown in Fig. 11. In the communication system, converter A operates as a transmitter while converter B acting as a receiver. The transmitter sends out bit "1" and "0" alternatively. In this way, the 50 kHz carrier presents when the transmitter is sending "1" and absents when sending "0." In the receiver, the carrier is sampled and a sliding discrete Fourier transformation (DFT) algorithm is employed [22], which is expressed by

$$X(k) = \sum_{n=0}^{N-1} x(n) e^{-j\frac{2\pi}{N}nk},\ k = 0, 1, \ldots, N-1) \qquad (33)$$

where $X(k)$ is the DFT result with kth harmonic, $x(n)$ is a discrete sequence in a period of DFT sliding window, and N is the sample number in a sliding window. To demodulate the signal, only carrier component should be calculated, so k equals to the carrier period number in a period of sample window $T_{\rm sp}$. In this experiment, $T_{\rm sp} = 100\ \mu$s, so $k = 5$.

The waveforms and the bit stream are shown in Fig. 14. The wire length in the experiment is about 10 m long. The upper figures are the waveform of transmission current and ripple voltage sampled by converter B, and the lower figures are the sliding window DFT calculation results. The amplitude of the DFT result represents the received signal voltage or the intensity of the data carrier.

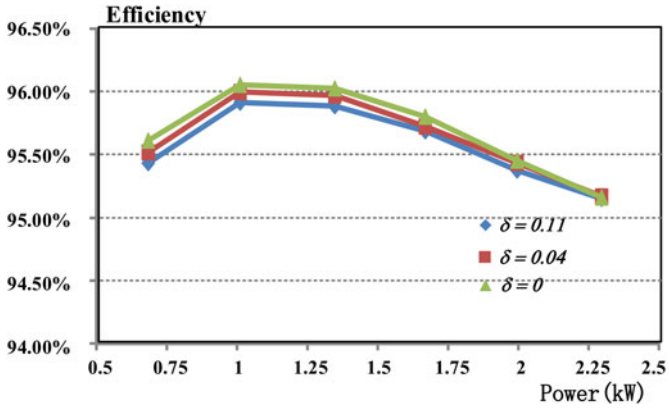

Fig. 15. Efficiency comparison with different perturbation depth.

Based on the DFT algorithm illustrated earlier, the existence or absence of the carrier is determined by comparing with a threshold; thus, data can be decoded. A 5 kbps communication is realized with the proposed method. In addition, it can be seen that, by modulating the perturbation depth, the signal intensity is regulated.

3) Impact on Conversion Efficiency: As shown in Figs. 12 and 14, the harmonics of the output current is enhanced with the increase of perturbation depth. This phenomenon raises the concern about the conversion efficiency of the circuit.

In the experiment, data are transmitted under different perturbation depth, the efficiency of the converter is measured by an accurate power analyzer (YOKOGAWA WT3000) and the result is shown in Fig. 15. It shows that, by the nature of introducing new harmonics, the efficiency of the converters decreases slightly. It should be noted that, even though the efficiency loss caused by data modulation is less than 0.3%, it may not be acceptable for some applications.

4) Influence of the Transmission Line: With the transmission length extended longer, the amplitude of the data signal is attenuated. In this experiment, the distance between the two PSFB converters is extended to 100 m. The cable is a stranded copper wire with 4 mm^2 cross-sectional area. The loop resistor of the cable is 1.8 Ω, and the inductance is about 57 μH, so the impedance at 50 kHz is about 18 Ω. As shown in Fig. 11(b), with a 5 μH inductor connected in series, the input impedance of the converter at 50 kHz is about 1.6 Ω. According to (25), the attenuation rate from the transmitter to the receiver is about 0.08.

The waveforms sampled and decoded in converter A (the transmitter) and converter B (the receiver) are shown in Fig. 16. When $\delta = 0.04$, the maximum value of the DFT result at converter A is about 0.24 V, which is consistent with the result previously. Meanwhile, the maximum value of the DFT result calculated in converter B is about 0.02 V due to signal attenuation, as shown in Fig. 16(a). In this case, signal is so small that it is hard to be recognized.

To increase the reliability of communication under this circumstance, larger perturbation depth should be employed, so as to increase the SNR of the signal received by converter B. In the

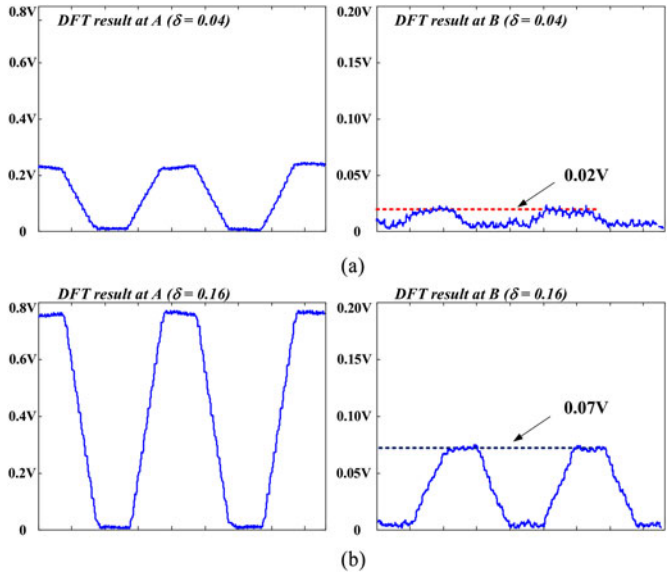

Fig. 16. Signal attenuation on 100 m transmission line: (a) with $\delta = 0.04$ and (b) with $\delta = 0.16$.

experiment, set $\delta = 0.16$, then the maximum value of the DFT result at site B increases to 0.072 V, by which the data can be recognized.

These results show that the proposed method can regulate the data carrier amplitude, which is a favorable feature in applications.

From the view of open system interconnection (OSI) model, the proposed method realizes bit-level communication in physical layer. To implement the communication system practically, media access control (MAC) layer should be employed. In this layer, many strategies such as master/slave mode and token ring protocol are the candidates. The master/slave mode is a simple method, but it has the drawback that if the master converter fails, the whole system will break down. To solve this problem, an improved master/slave mode strategy can be employed. In this method, a master converter dominates the communication channel and communicates with the slaves in turn. However, the master converter is not predetermined by address but dynamically determined by competition according to the output current, that means the master is always the converter which sends out maximum current. According to this strategy, if the master converter fails, the converter with second-maximum output current will become a new master automatically. In this way, the failure of the master converter would not influence the validity of the communication system. More details about communication protocols are beyond the scope of this paper and are not be discuss here.

V. Conclusion

This paper presents an improved dc power-line communication approach implemented using the PSDM in PSFB converters. Comparing with the conventional PLC solutions, this method has the advantages of embedding the communication in the power conversion circuit without using extra wiring and coupling units and a simplified system structure. These advantages are attained by introducing a phase-based freedom in conventional power control loop of a PSFB converter. In addition, with the proposed perturbation depth, the signal intensity in this method can be regulated to adapt to different operating conditions. The testing of the proposed method has been performed in a 2 kW prototype system, where a 5 kbps communication link is implemented and the method is verified.

Although the proposed method provides a low-cost approach to meet the communication need in a DC-DPS, it has constraints in the following aspects. First, the data carrier signal can only be injected upon the output line of a converter with this method. For a DC-DPS consisting of both generation converters and load converters, only the generation converters can send out information. Second, the communication may be influenced by current harmonics happen to have the same frequency with the data carrier, produced by any converter connected to the bus. So this method is more suitable for the DC-DPS applications that all the converters are preconditioned.

References

[1] C. D. Xu and K. W. E. Cheng, "A survey of distributed power system—AC versus DC distributed power system," in *Proc. Int. Conf. Power Electron. Syst. Appl.*, 2011, pp. 1–12.

[2] F. Blaabjerg, R. Teodorescu, M. Liserre, and A. V. Timbus, "Overview of control and grid synchronization for distributed power generation systems," *IEEE Trans. Ind. Electron.*, vol. 53, no. 5, pp. 1398–1409, Jan. 2006.

[3] J. M. Carrasco, L. G. Franquelo, L. T. Bialasiewicz, E. Galvan, P. C. P. Guisado, M. A. M. Prats, J. I. Leon, and N. Moreno-Alfonso, "Power-electronic systems for the grid integration of renewable energy sources: A survey," *IEEE Trans. Ind. Electron.*, vol. 53, no. 4, pp. 1002–1016, Aug. 2006.

[4] S. Luo and I. Batarseh, "A review of distributed power systems part I: DC distributed power system," *IEEE Aerosp. Electron. Syst. Mag.*, vol. 20, no. 8, pp. 5–16, Aug. 2005.

[5] A. Yadav and L. Srivastava, "Optimal placement of distributed generation: An overview and key issues", in *Proc. Int. Conf. Power Signals Con. Comput.*, 2014, pp. 1–6.

[6] E. Serban and H. Serban, "A control strategy for a distributed power generation microgrid application with voltage- and current-controlled source converter," *IEEE Trans. Power Electron.*, vol. 25, no. 12, pp. 2981–2992, Dec. 2010.

[7] A. V. Timbus, M. Liserre, R. Teodorescu, P. Rodriguez, and F. Blaabjerg, "Evaluation of current controllers for distributed power generation systems," *IEEE Trans. Power Electron.*, vol. 24, no. 3, pp. 654–664, Mar. 2009.

[8] R. Lasseter, "Microgrids," in *Proc. IEEE-PES Winter Meeting*, Jan. 2002, vol. 1, pp. 305–308.

[9] S. P. Engel, M. Stieneker, N. Soltau, S. Rabiee, H. Stagge, and R. W. De Doncker, "Comparison of the modular multilevel DC converter and the dual-active bridge converter for power conversion in HVDC and MVDC grids," *IEEE Trans. Power Electron.*, vol. 30, no. 1, pp. 124–137, Jan, 2015.

[10] A. Nami, L. Jiaqi, F. Dijkhuizen, and G. D. Demetriades, "Modular multilevel converters for HVDC applications: Review on converter cells and functionalities," *IEEE Trans. Power Electron.*, vol. 30, no. 1, pp. 18–36, Jan. 2015.

[11] M. Guan and Z. Xu, "Modeling and control of a modular multilevel converter-based HVDC system under unbalanced grid conditions," *IEEE Trans. Power Electron.*, vol. 27, no. 12, pp. 4858–4867, Dec. 2012.

[12] V. Nasirian, S. Moayedi, A. Davoudi, and F. Lewis, "Distributed cooperative control of DC microgrids," *IEEE Trans. Power Electron.*, vol. 30, no. 4, pp. 2288–2303, Apr. 2015.

[13] M. Farhadi and O. A. Mohammed, "Real-time operation and harmonic analysis of isolated and non-isolated hybrid DC microgrid," *IEEE Trans. Ind. Appl.*, vol. 50, no. 4, pp. 2900–2909, Jul./Aug. 2014.

[14] N. Eghtedarpour and E. Farjah, "Power control and management in a hybrid AC/DC microgrid," *IEEE Trans. Smart Grid*, vol. 5, no. 3, pp. 1494–1505, May 2014.
[15] D. Chen, L. Xu, and L. Yao, "DC voltage variation based autonomous control of DC microgrids," *IEEE Trans. Power Del.*, vol. 28, no. 2, pp. 637–648, Apr. 2013.
[16] P. Karlsson and J. Svensson, "DC bus voltage control for a distributed power system," *IEEE Trans. Power Electron.*, vol. 18, no. 6, pp. 1405–1412, Nov. 2003.
[17] X. Lu, J. M. Guerrero, K. Sun, and J. C. Vasquez, "An improved droop control method for dc microgrids based on low bandwidth communication with dc bus voltage restoration and enhanced current sharing accuracy," *IEEE Trans. Power Electron.*, vol. 29, no. 4, pp. 1800–1812, Apr. 2014.
[18] V. Kounev, D. Tipper, B. M. Grainger, and G. Reed. "Analysis of an offshore medium voltage DC microgrid environment part II: Communication network architecture," in *Proc IEEE/PES Trans. Distrib. Conf. Expo.*, pp. 1–5, Apr. 2014.
[19] Y. Li, F. Liu, L. Lyo, C. Rehtanz, and Y. Cao, "Enhancement of commutation reliability of an HVDC inverter by means of an inductive filtering method," *IEEE Trans. Power Electron.*, vol. 28, no. 11, pp. 4917–4929, Nov. 2013.
[20] A. Pinomaa, J. Ahola, and A. Kosonen, "Power-line communication based network architecture for LVDC distribution system," in *Proc. 2011 IEEE Int. Symp. Power Line Commun. Appl.*, Udine, Italy, pp. 358–363.
[21] A. Pinomaa, J. Ahola, and A. Kosonen, "PLC concept for LVDC distribution systems," *IEEE Commun. Mag.*, vol. 49, no. 12, pp. 55–63, Dec. 2011.
[22] J. Wu, J. Du, Z. Lin, Y. Hu, C. Zhao, and X. He, "Power conversion and signal transmission integration method based on dual modulation of DC-DC converters," *IEEE Trans. Ind. Electron.*, vol. 62, no. 2, pp. 1291–1300, Feb. 2015.
[23] G. D. Capua, S. A. Shirsavar, M. A. Hallworth, and N. Femia, "An enhanced model for small-signal analysis of the phase-shifted full-bridge converter," *IEEE Trans. Power Electron.*, vol. 30, no. 3, pp. 1567–1576, Mar. 2015.
[24] W. Chen, X. Ruan, H. Yan, and C. K. Tse, "DC/DC conversion systems consisting of multiple converter modules: Stability, control and experimental verifications," *IEEE Trans. Power Electron.*, vol. 24, no. 6, pp. 1463–1474, Jun. 2009.
[25] J. H. Cho, K. B. Park, J. S. Park, G. W. Moon, and M. J. Youn, "Design of a digital offset compensator eliminating transformer magnetizing current offset of a phase-shift full-bridge converter," *IEEE Trans. Power Electron.*, vol. 27, no. 1, pp. 331–341, Jan. 2012.
[26] X. Wu, H. Chen, J, Zhang, F. Peng, and Z. Qian, "Interleaved phase-shift full-bridge converter with transformer winding series–parallel auto regulated (SPAR) current doubler rectifier," *IEEE Trans. Power Electron.*, vol. 30, no. 9, pp. 4864–4873, Sep. 2015.

Jin Du (S'11) received the B.S. degree in electrical engineering, in 2011, from Zhejiang University, Hangzhou, China, where he is currently working toward the Ph.D. degree in the College of Electrical Engineering.

His current research interests include power optimization of renewable generation and communication technique applied in power electronics.

Jiande Wu (M'11) was born in Zhejiang, China, in 1973. He received the B.Sc., M.Sc., and Ph.D. degrees from the College of Electrical Engineering, Zhejiang University, Hangzhou, China, in 1994, 1997, and 2012, respectively.

Since 1997, he has been a Faculty Member at Zhejiang University, where he is currently an Associate Professor. From 2013 to 2014, he was an Academic Visitor at the University of Strathclyde, Glasgow, U.K. His current research interests include power electronics control, distributed power electronics system, and fieldbus communication.

Ruichi Wang received the B.S. degree in electrical engineering, in 2013, from Zhejiang University, Hangzhou, China, where she is currently working toward the Ph.D. degree in the College of Electrical Engineering.

Her current research interests include communication technique applied in power electronics and EMI mitigation for SMPS.

Zhengyu Lin (S'03–M'05–SM'10) received the B.Sc. and M.Sc. degrees from the College of Electrical Engineering, Zhejiang University, Hangzhou, China, in 1998 and 2001, respectively, and the Ph.D. degree from Heriot-Watt University, Edinburgh, U.K., in 2005.

He is currently a Lecturer in the Electrical, Electronic, and Power Engineering with Aston University, Birmingham, U.K. He was a Research Associate with the University of Sheffield from 2004 to 2006, an R&D Engineer with Emerson Industrial Automation, Control Techniques PLC from 2006 to 2011, a Senior Research Scientist with Sharp Laboratories of Europe Ltd., from 2011 to 2012, and a Lecturer with Coventry University from 2013 to 2014. His current research interests include power electronics and its applications in renewable energy, energy storage, motor drives, and power systems.

Xiangning He (M'95–SM'96–F'10) received the B.Sc. and M.Sc. degrees from Nanjing University of Aeronautical and Astronautical, Nanjing, China, in 1982 and 1985, respectively, and the Ph.D. degree from Zhejiang University, Hangzhou, China, in 1989.

From 1985 to 1986, he was an Assistant Engineer at the 608 Institute of Aeronautical Industrial General Company, Zhuzhou, China. From 1989 to 1991, he was a Lecturer at Zhejiang University. In 1991, he obtained a Fellowship from the Royal Society of U.K. and conducted research in the Department of Computing and Electrical Engineering, Heriot-Watt University, Edinburgh, U.K., as a Post-Doctoral Research Fellow for two years. In 1994, he joined Zhejiang University as an Associate Professor, where since 1996, he has been a Full Professor in the College of Electrical Engineering, Zhejiang University. He was the Director of the Power Electronics Research Institute and the Head of the Department of Applied Electronics. He is currently the Vice Dean of the College of Electrical Engineering, Zhejiang University. His current research interests include power electronics and their industrial applications. He is the author or coauthor of more than 280 papers and one book *Theory and Applications of Multi-level Converters*. He holds 22 patents.

Dr. He received the 1989 Excellent Ph.D. Graduate Award, the 1995 Elite Prize Excellence Award, the 1996 Outstanding Young Staff Member Award and 2006 Excellent Staff Award from Zhejiang University for his teaching and research contributions. He received seven Scientific and Technological Achievements Awards from Zhejiang Provincial Government and the State Educational Ministry of China in 1998, 2002, 2009 and 2011 respectively, and six Excellent Paper Awards. He has been appointed as the IEEE Distinguished Lecturer by the IEEE Power Electronics Society in 2011. He is also a Fellow of the Institution of Engineering and Technology (formerly IEE), U.K.